Acknowledgment. This work was supported by the National Science and Engineering Research Council of Canada in the form of operating grants to W.R.C. and F.W.B.E.

Registry No. I, 67124-61-2; II, 75010-83-2; III, 72765-07-2; IV, 75010-84-3; V, 75024-08-7; VI, 75010-86-5; $Fe(CO)_5$, 13463-40-6; $Fe_3(CO)_{12}$, 17685-52-8.

Supplementary Material Available: Tables of the observed and calculated structure factors for both isomers (29 pages). Ordering information is given on any current masthead page.

Contribution from the Department of Chemistry, University of Minnesota, Minneapolis, Minnesota 55455

Photochemical Properties and X-ray Structural Characterization of a Tetranuclear Bimetallic Complex: $[Rh_2(TM4\text{-bridge})_4Mn_2(CO)_{10}](PF_6)_2 \cdot 2(CH_3)_2CO$ (TM4-bridge = 2,5-Dimethyl-2,5-diisocyanohexane)

DAVID A. BOHLING, THOMAS P. GILL, and KENT R. MANN*

Received June 18, 1980

The sunlight irradiation of $Mn_2(CO)_{10}$ in the presence of $Rh_2(TM4\text{-bridge})_4PF_6$ (TM4-bridge = 2,5-dimethyl-2,5-diisocyanohexane) in acetone solution yields the mixed-metal tetranuclear compound $[Rh_2(TM4\text{-bridge})_4Mn_2(CO)_{10}](PF_6)_2 \cdot 2(CH_3)_2CO$. The dark green crystals obtained from acetone/hexane crystallize in the space group *Pna*2 (No. 33) (a = 18.265 (11), b = 23.185 (7), c = 17.836 (4) Å; Z = 4, ρ(calcd) = 1.391 (1), ρ(obsd) = 1.41 (2) g/cm^3). The structure is composed of tetranuclear $[(CO)_5MnRh_2(TM4\text{-bridge})_4Mn(CO)_5]^{2+}$ cations having approximate D_{2d} symmetry, PF_6^- anions, and two acetone molecules of crystallization per formula unit. The geometry about each Mn and Rh atom is approximately pseudooctahedral. The RhRh bond length is 2.922 (2) Å while the two RhMn bonds are 2.905 (5) and 2.883 (4) Å. The quantum yields for the formation of $[Rh_2(TM4\text{-bridge})Mn_2(CO)_{10}]^{2+}$ in acetone solution (2.6×10^{-3} M in $Mn_2(CO)_{10}$ and 1.2×10^{-3} M in $Rh_2(TM4\text{-bridge})_4^{2+}$) were measured by irradiation with 405- and 546-nm light. At 405 nm, the quantum yield for the formation of $[Rh_2(TM4\text{-bridge})_4Mn_2(CO)_{10}]^{2+}$ (a wavelength corresponding to absorbance by $Mn_2(CO)_{10}$) was ϕ = 0.20 (1). At 546 nm, where greater than 99% of the light is absorbed by $Rh_2(TM4\text{-bridge})_4^{2+}$, the quantum yield was found to be $\phi \approx 3\ (1) \times 10^{-4}$, almost 3 orders of magnitude smaller than at 405 nm. These data are tentatively interpreted in terms of the generation of $Mn(CO)_5$ radicals which are efficiently collected by the $Rh_2(TM4\text{-bridge})_4^{2+}$ ion present in solution. The $[Rh_2(TM4\text{-bridge})_4Mn_2(CO)_{10}]^{2+}$ ion was found to be relatively stable in degassed acetone solution under photolysis with a 4-mW HeNe laser ($\phi_{decomposition} \approx 5\ (2) \times 10^{-5}$). In the presence of oxygen, however, irradiation of the complex regenerates $Rh_2(TM4\text{-bridge})_4^{2+}$ ($\phi_{decomposition} \approx 2\ (1) \times 10^{-2}$) and an undetermined Mn complex. These properties are discussed in terms of simple molecular orbital theory.

There has been much recent interest[1] in the synthesis and properties of metal cluster compounds as candidates for catalyzing potentially useful reactions. Of interest to us has been the synthesis of mixed-metal cluster compounds which incorporate the potential to serve as photoassistance agents utilizing visible radiation for the initiation of the photoassistance cycle. As our visible-light-absorbing chromophore, we have chosen to investigate compounds which contain $\sigma \rightarrow \sigma^*$ transitions due to the metal–metal bonds contained in the molecule. Our hope was to extend the metal–metal interaction to multiple metal centers, so as to move the $\sigma \rightarrow \sigma^*$ transitions from the near-ultraviolet[2] into the visible spectral region. Second, we hope that similar photochemical reactions as found in binuclear systems (i.e., metal–metal bond cleavage[3]) could be induced, photogenerating reactive intermediates which could be used as the catalytic agents in the photoassistance cycle.

We now wish to report the synthesis, X-ray structure determination, and a preliminary photochemical investigation of a linear tetranuclear cluster containing Rh and Mn, which represents our initial attempt at producing a cluster with the properties which we feel will be useful in visible-light photoassistance schemes.

Experimental Section

General Information. The synthesis of the starting material $Rh_2(TM4\text{-bridge})_4(PF_6)_2$ (TM4-bridge = 2,5-dimethyl-2,5-diisocyanohexane) has been reported previously.[4] $Mn_2(CO)_{10}$ was purchased from ROC/RIC. The solvents used were of spectroscopic quality. IR, NMR, and UV–vis spectra were obtained by using a Perkin-Elmer 283, a Varian Associates CFT 20 equipped with a 79.5-MHz proton accessory, and a Cary 17D spectrophotometer, respectively. The elemental analyses were performed at Galbraith Laboratories, Knoxville, Tenn.

Preparation of $[Rh_2(TM4\text{-bridge})_4Mn_2(CO)_{10}](PF_6)_2 \cdot 2(CH_3)_2CO$. A sample of 81.1 mg of $Rh_2(TM4\text{-bridge})_4(PF_6)_2$ (0.0707 mmol) and 84.7 mg of $Mn_2(CO)_{10}$ (0.271 mmol) in 20 mL of acetone were placed along with a stir bar in a Pyrex test tube sealed with a serum stopper and degassed by a N_2 purge for 20 min. The resulting bright red solution was then stirred in bright Minneapolis sunshine at ambient temperature. Immediately, on exposure to sunlight, the solution turned a dark royal blue color and was stirred for an additional 1.5 h. The solution was evaporated to dryness on a rotary evaporator and washed several times with hexane to remove the remaining excess $Mn_2(CO)_{10}$. Recrystallization of the residue from acetone/hexane afforded 93.4 mg (0.0565 mmol) of $[Rh_2(TM4\text{-bridge})_4Mn_2(CO)_{10}](PF_6)_2 \cdot 2(CH_3)_2CO$, an 80% yield (based on the Rh complex). Anal. Calcd for $Rh_2Mn_2C_{56}H_{70}N_8O_{12}P_2F_{12}$: C, 40.69; H, 4.27; N, 6.78. Found: C, 40.40; H, 4.41; N, 6.81. Mp: 175 °C dec (sealed capillary). NMR spectrum (acetone-d_6): CH_3, acetone of crystallization, τ 7.92; CH_3, TM4-bridge, τ 8.37 (br, s); CH_2, TM4-bridge, τ 8.25 (br, s). IR spectrum (acetone solution): $\bar{\nu}$(CN) 2178 cm^{-1} (vs), $\bar{\nu}$(CO) 2038 cm^{-1}

(1) (a) Moskovits, M. *Acc. Chem. Res.* **1979**, *12*, 229–236. (b) Muetterities, E. L.; Rhodin, T. N.; Band, E.; Brucker, C. F.; Pretzer, W. R. *Chem. Rev.* **1979**, *79*, 91–138. (c) Muetterties, E. L. *Ibid.* **1978**, *78*, 639–658 and references contained therein.
(2) Levenson, R. A.; Gray, H. B. *J. Am. Chem. Soc.* **1975**, *97*, 6042–6047.
(3) (a) Wrighton, M. S. *Top. Curr. Chem.* **1976**, *37*, 69–78. (b) Geoffroy, G. L.; Wrighton, M. S. "Organometallic Photohemistry"; Academic Press: New York, 1979; pp 136–141 and references therein.
(4) (a) Mann, K. R.; Thich, J. A.; Bell, R. A.; Coyle, C. L.; Gray, H. B. *Inorg. Chem.*, in press. (b) Mann, K. R.; Gray, H. B. *Adv. Chem. Ser.* **1979**, *No. 173*, 225–235.

0020-1669/81/1320-0194$01.00/0

Table I. Crystal Data for $[Rh_2(TM4\text{-bridge})_4Mn_2(CO)_{10}](PF_6)_2 \cdot 2(CH_3)_2CO$

fw 1582.29	$V = 7553.1$ (85) Å^3
space group $Pna2_1$	ρ(calcd) = 1.39 (1) g/cm^3
$a = 18.265$ (11) Å	ρ(obsd) = 1.41 (2) g/cm^3
$b = 23.185$ (7) Å	$\lambda = 0.710\ 73$ Å (Mo Kα)
$c = 17.836$ (4) Å	temp = 22 (1) °C
$Z = 4$	$\mu = 8.909$ cm^{-1}

(vs), 1978 cm^{-1} (vs). UV–Vis spectrum (acetone solution): λ_{max} = 600 nm, ϵ_{max} = 106 000 ± 6000 M^{-1} cm^{-1}.

Photochemical Measurements. Photolyses for quantum yield measurements were carried out (405 and 546 nm) by isolating these lines (interference filters) from the output of an Oriel Model 6281 100-W mercury lamp or (632.8 nm) by directly using the output from a 4-mW HeNe laser.

Quantum yields were determined at 20 ± 1 °C by photolysis of acetone solutions in cells which could be degassed by freeze/pump/thaw cycles. Analyses of the extent of reaction were made spectrophotometrically. Actinometry was carried out at 405 and 546 nm by using Reinecke's salt.[5] The light intensities were typically 2.8×10^{-6} einstein min^{-1} and 4.7×10^{-6} einstein min^{-1}, respectively. The output at 632.8 nm from the 4-mW HeNe laser was assumed to be 1.27×10^{-6} einstein min^{-1}. The quantum yields reported here have been corrected for incomplete light absorption.[6]

Collection and Reduction of the Crystallographic Data. The crystal selected was a well-formed prism of approximate dimensions 0.2 × 0.2 × 0.3 mm. This crystal was sealed in a capillary to minimize any potential loss of solvent. The automatic peak searching, centering, and indexing routines available on the Enraf-Nonius SDP-CAD4 automatic diffractometer[7] were used to find and center 25 reflections which were used to define the unit cell constants. The space group $Pna2_1$ was assigned by examining the data for systematic absences and was subsequently successfully employed in solving and refining the structure. Crystal data are given in Table I. The density, ρ = 1.41 (2) g cm^{-3}, measured by the flotation method in CCl_4/hexane is in close agreement with the calculated value of 1.391 (1) g cm^{-1} for $Z = 4$. A total of 7284 independent reflections were collected in the scan range 2θ = 0–50° with use of graphite monochromatized Mo Kα radiation by employing the ω–2θ scan technique. Crystal decomposition was monitored by three check reflections collected every 75 reflections. No decay or significant fluctuation was observed during data collection. After data processing and reduction,[8] 2906 reflections, for which $F_o^2 > 3.0\sigma(F_o^2)$, were used in the structure solution and refinement. No correction was made for absorption (μ = 8.909 cm^{-1}).

The structure was solved from the three-dimensional Patterson function which allowed placement of the Rh and Mn atoms. Fourier and difference Fourier analyses in conjunction with cycles of least-squares refinement[9] allowed the placement of the remaining atoms, excluding the hydrogens. Full-matrix least-squares refinement utilizing anisotropic temperature factors for Rh and Mn and isotropic temperature factors for C, N, O, P, and F (396 variables) converged to

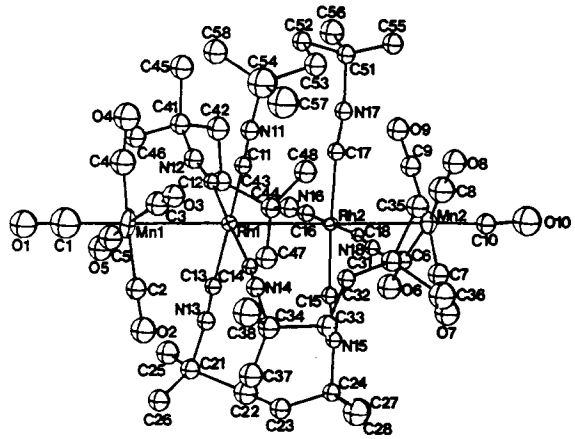

Figure 1. ORTEP drawing of the $[Rh_2(TM4\text{-bridge})_4Mn_2(CO)_{10}]^{2+}$ dication showing the labeling scheme.

give an R and R_w of 0.072 and 0.093, respectively. Scattering factors were from Cromer and Waber;[10] the effects of anomalous dispersion were included.[11] The error in an observation of unit weight was 1.82 with the use of a value of 0.08 for p in the $\sigma(I)$ equation.[8] A final difference Fourier revealed no significant features, except those due to residual electron density due to the hydrogen positions which were not included in any of the calculations. Table II contains the final positional and thermal parameters, while a list of final calculated and observed structure factors is available.

Results and Discussion

Structure of $[Rh_2(TM4\text{-bridge})_4Mn_2(CO)_{10}](PF_6)_2 \cdot 2(CH_3)_2CO$. Exposure of solutions which contain $Mn_2(CO)_{10}$ and $Rh_2(TM4\text{-bridge})_4(PF_6)_2$ to sunlight results in the efficient and high overall conversion to the tetranuclear complex cation $[Rh_2(TM4\text{-bridge})_4Mn_2(CO)_{10}]^{2+}$, which is a royal blue color in acetone solution. An X-ray crystallographic analysis of the PF_6^- salt was carried out to determine the structure of the complex cation.

The compound $[Rh_2(TM4\text{-bridge})_4Mn_2(CO)_{10}](PF_6)_2 \cdot 2(CH_3)_2CO$ crystallizes in the $Pnma2_1$ space group with 4 formula weights per unit cell. The $[Rh_2(TM4\text{-bridge})_4Mn_2(CO)_{10}]^{2+}$ cation having approximate D_{2d} symmetry is best described as a $Rh_2(TM4\text{-bridge})_4^{2+}$ unit having D_{2d} symmetry capped on each end by a $Mn(CO)_5$ unit. (See Figures 1 and 2; bond lengths and bond angles are given in Tables III–V.) The RhRh bond length of 2.922 (2) Å is shorter than the Rh(I)Rh(I) bond (3.264 (1) Å) in the parent compound $Rh_2(TM4\text{-bridge})_4(PF_6)_2 \cdot CH_3CN$ by over 0.3 Å,[4] consistent with the formation of a much stronger bonding interaction between the Rh atoms in the Mn derivative. In another tetranuclear compound which has been recently determined[12] and which contains the $[Rh_4(bridge)_8Cl]^{5+}$ ion (bridge = 1,3 diisocyanopropane) the central RhRh distance was found to be somewhat shorter (2.775 (4) Å). The RhMn bond lengths of 2.905 (5) Å for Rh1Mn1 and 2.883 (4) Å for Rh2Mn2 are almost identical and also very similar to the Rh1Rh2 bond length. The MnMn bond length in $Mn_2(CO)_{10}$[13] of 2.923 (3) is also seen to be close to this value. In another compound which consists of a square-planar $Fe(CO)_4$ unit capped on each side by a $Mn(CO)_5$ unit ($Mn_2Fe(CO)_{14}$)[14] the MnFe distances

(5) Wegner, E. E.; Adamson, A. W. *J. Am. Chem. Soc.* **1966**, *88*, 394–404.
(6) Kling, O.; Nikoaiski, E.; Schläfer, H. L. *Ber. Bunseges. Phys. Chem.* **1963**, *67*, 883–892.
(7) All calculations were carried out on PDP 8A and 11/34 computers using the Enraf-Nonius CAD 4-SDP programs. This crystallographic computing package is described by: Frenz, B. A. In "Computing in Crystallography"; Schenk, H., Olthof-Hazekamp, R., van Koningsveld, H., Bassi, G. C., Eds.; Delft University Press: Delft, Holland, 1978; pp 64–71. "CAD 4 SDP Users Manual"; Enraf-Nonius: Delft, Holland, 1978.
(8) The intensity data were processed as described in: "CAD 4 and SDP Users Manual"; Enraf-Nonius: Delft, Holland, 1978. The net intensity I is given as $I = (K/\text{NPI})(C - 2B)$, where $K = 20.1166x$ (attenuator factor), NPI = ratio of fastest possible scan rate to scan rate for the measurement, C = total count, and B = total background count. The standard deviation in the net intensity is given by $\sigma^2(I) = (K/\text{NPI})[C + 4B + (pI)^2]$, where p is a factor used to downweight intense reflections. The observed structure factor amplitude F_o is given by $F_o = (I/Lp)^{1/2}$, where Lp = Lorentz and polarization factors. The $\sigma(I)$'s were converted to the estimated errors in the relative structure factors $\sigma(F_o)$ by $\sigma(F_o) = {}^1/_2(\sigma(I)/I)F_o$.
(9) The function minimized was $\sum w(|F_o| - |F_c|)^2$, where $w = 1/\sigma^2(F_o)$. The unweighted and weighted residuals are defined as $R = (\sum||F_o| - |F_c||)/\sum|F_o|$ and $R_w = [(\sum w(|F_o| - |F_c|))^2/(\sum w|F_o|^2)]^{1/2}$. The error in an observation of unit weight is $[\sum w(|F_o| - |F_c|)^2/(NO - NV)]^{1/2}$, where NO and NV are the number of observations and variables, respectively.
(10) Cromer, D. T.; Waber, J. T. "International Tables for X-ray Crystallography"; Kynoch Press: Birmingham, England, 1974; Vol. IV, Table 2.2.4. Cromer, D. T. *Ibid.*; Kynoch Press: Birmingham, England, 1974; Vol. IV, Table 2.3.1.
(11) Cromer, D. T.; Ibers., J. A. "International Tables for X-ray Crystallography"; Kynoch Press: Birmingham, England, 1974; Vol. IV.
(12) Mann, K. R.; DiPierro, M. J.; Gill, T. P. *J. Am. Chem. Soc.* **1980**, *102*, 3965–3967.
(13) Dahl, L. F.; Rundle, R. E. *Acta Crystallogr.* **1963**, *16*, 419–426.
(14) Argon, P. A.; Ellison, R. D.; Levy, H. A. *Acta Crystallogr.* **1967**, *23*, 1079–1086.

Table II. Positional, Thermal, and Anisotropic Thermal Parameters and Their Estimated Standard Deviations[a]

atom	x	y	z	B, Å²	atom	x	y	z	B, Å²
Rh(1)	0.24085 (10)	0.00672 (8)	−0.0580 (0)		C(10)	0.233 (2)	0.2130 (12)	0.267 (2)	5.6 (7)
Rh(2)	0.23831 (9)	0.09059 (8)	0.0643 (1)		C(11)	0.337 (1)	0.0289 (11)	−0.080 (2)	4.3 (6)
Mn(1)	0.2418 (3)	−0.0774 (2)	−0.1787 (3)		C(12)	0.284 (1)	−0.0494 (12)	0.013 (1)	3.3 (5)
Mn(2)	0.2365 (3)	0.1684 (2)	0.1903 (3)		C(13)	0.138 (1)	−0.0204 (11)	−0.030 (2)	3.9 (6)
P(1)	0.2408 (5)	0.4505 (4)	0.0358 (5)	6.1 (2)	C(14)	0.197 (1)	0.0655 (11)	−0.126 (1)	3.4 (5)
P(2)	−0.0735 (7)	0.2511 (6)	−0.3263 (7)	10.2 (4)	C(15)	0.134 (1)	0.0970 (10)	0.060 (2)	3.7 (5)
F(11)	0.295 (1)	0.4520 (10)	0.104 (1)	10.3 (7)	C(16)	0.233 (1)	0.0286 (11)	0.135 (1)	3.9 (6)
F(12)	0.288 (1)	0.4012 (9)	0.013 (1)	8.9 (6)	C(17)	0.347 (1)	0.0888 (12)	0.070 (2)	4.3 (5)
F(13)	0.191 (1)	0.4115 (12)	0.084 (2)	13.4 (8)	C(18)	0.244 (1)	0.1561 (9)	−0.005 (1)	2.4 (4)
F(14)	0.308 (1)	−0.0002 (11)	−0.441 (2)	12.8 (8)	C(21)	0.004 (2)	−0.0543 (13)	−0.003 (2)	5.3 (7)
F(15)	0.291 (2)	0.4900 (13)	−0.016 (2)	14.4 (9)	C(22)	−0.026 (2)	0.0032 (17)	0.041 (2)	8.2 (10)
F(16)	0.185 (1)	0.4357 (11)	−0.031 (2)	13.1 (8)	C(23)	−0.034 (2)	0.0645 (13)	0.006 (2)	5.9 (8)
F(21)	−0.081 (2)	0.1817 (14)	−0.314 (2)	18.7 (12)	C(24)	−0.008 (1)	0.1109 (11)	0.053 (2)	4.4 (6)
F(22)	−0.007 (2)	0.7627 (15)	0.156 (2)	20.0 (14)	C(25)	0.011 (2)	−0.1058 (14)	0.047 (2)	7.1 (9)
F(23)	0.106 (3)	0.7634 (23)	0.107 (3)	29.4 (22)	C(26)	−0.035 (2)	−0.0628 (13)	−0.076 (2)	6.3 (8)
F(24)	0.646 (3)	−0.2409 (22)	0.210 (3)	30.7 (21)	C(27)	−0.044 (2)	0.1191 (17)	0.126 (2)	8.1 (10)
F(25)	0.050 (3)	0.7565 (18)	0.262 (3)	26.0 (18)	C(28)	−0.019 (2)	0.1688 (18)	−0.003 (2)	10.2 (13)
F(26)	0.074 (3)	0.6843 (21)	0.153 (3)	27.9 (21)	C(31)	0.235 (2)	0.2409 (13)	−0.098 (2)	5.7 (7)
O(1)	0.243 (1)	−0.1641 (11)	−0.305 (2)	10.5 (8)	C(32)	0.214 (1)	0.2145 (11)	−0.175 (2)	4.5 (6)
O(2)	0.097 (1)	−0.0321 (10)	−0.216 (1)	8.9 (7)	C(33)	0.142 (2)	0.1958 (13)	−0.182 (2)	6.2 (8)
O(3)	0.315 (1)	0.0167 (9)	−0.267 (1)	6.9 (6)	C(34)	0.133 (2)	0.1347 (14)	−0.220 (2)	6.6 (8)
O(4)	0.390 (1)	−0.1093 (12)	−0.128 (2)	10.1 (8)	C(35)	0.322 (2)	0.2706 (14)	−0.097 (2)	7.1 (9)
O(5)	0.174 (1)	−0.1581 (10)	−0.065 (1)	8.5 (6)	C(36)	0.189 (2)	0.2958 (17)	−0.061 (2)	9.9 (12)
O(6)	0.118 (1)	0.0966 (10)	0.253 (1)	8.1 (6)	C(37)	0.059 (2)	0.1166 (15)	−0.223 (2)	8.0 (10)
O(7)	0.127 (1)	0.2350 (11)	0.107 (1)	8.5 (7)	C(38)	0.166 (2)	0.1348 (19)	−0.294 (3)	11.1 (13)
O(8)	0.353 (1)	0.2301 (10)	0.110 (1)	7.9 (6)	C(41)	0.343 (2)	−0.1303 (13)	0.096 (2)	5.5 (7)
O(9)	0.354 (1)	0.0914 (9)	0.259 (1)	6.9 (5)	C(42)	0.328 (2)	−0.1131 (15)	0.177 (2)	7.1 (9)
O(10)	0.233 (2)	0.2413 (13)	0.330 (2)	11.8 (9)	C(43)	0.246 (2)	−0.1118 (12)	0.197 (2)	5.4 (7)
O(15)	0.011 (3)	0.2439 (21)	0.291 (4)	28.9 (25)	C(44)	0.210 (2)	−0.0586 (13)	0.232 (2)	5.5 (7)
O(25)	0.222 (3)	0.1192 (23)	0.408 (3)	22.9 (17)	C(45)	0.432 (2)	−0.1265 (15)	0.081 (2)	7.8 (10)
N(11)	0.395 (1)	0.0431 (10)	−0.100 (1)	5.0 (5)	C(46)	0.316 (2)	−0.1821 (14)	0.082 (2)	6.2 (8)
N(12)	0.305 (1)	−0.0903 (10)	0.050 (1)	5.3 (5)	C(47)	0.131 (2)	−0.0663 (14)	0.248 (2)	6.6 (8)
N(13)	0.082 (1)	−0.0308 (9)	−0.019 (1)	4.6 (5)	C(48)	0.257 (2)	−0.0458 (14)	0.304 (2)	7.0 (8)
N(14)	0.178 (1)	0.0932 (10)	−0.170 (1)	5.1 (5)	C(51)	0.491 (1)	0.0878 (12)	0.084 (2)	4.8 (7)
N(15)	0.069 (1)	0.1062 (8)	0.060 (1)	3.8 (4)	C(52)	0.515 (1)	0.0571 (12)	0.014 (2)	5.0 (7)
N(16)	0.227 (1)	−0.0133 (10)	0.181 (1)	5.6 (6)	C(53)	0.499 (2)	0.1048 (15)	−0.054 (2)	7.2 (9)
N(17)	0.407 (1)	0.0910 (9)	0.080 (1)	4.6 (5)	C(54)	0.472 (3)	0.0626 (20)	−0.118 (3)	12.5 (16)
N(18)	0.237 (1)	0.1920 (8)	−0.043 (1)	3.3 (4)	C(55)	0.517 (2)	0.1459 (14)	0.092 (2)	5.9 (8)
C(1)	0.242 (2)	−0.1327 (23)	−0.246 (3)	13.2 (16)	C(56)	0.505 (2)	0.0396 (15)	0.151 (2)	8.4 (10)
C(2)	0.153 (2)	−0.0502 (13)	−0.203 (2)	6.0 (8)	C(57)	0.463 (3)	0.1190 (22)	−0.185 (3)	13.8 (16)
C(3)	0.291 (2)	−0.0182 (16)	−0.231 (2)	8.0 (10)	C(58)	0.488 (2)	0.9926 (16)	0.358 (2)	8.0 (10)
C(4)	0.325 (2)	−0.1050 (17)	−0.140 (2)	9.3 (11)	C(15)	−0.017 (4)	0.2117 (30)	0.317 (4)	23.2 (26)
C(5)	0.201 (2)	−0.1283 (16)	−0.107 (2)	8.3 (10)	C(25)	0.024 (4)	0.2410 (29)	0.399 (5)	22.1 (29)
C(6)	0.166 (1)	0.1229 (12)	0.227 (2)	4.6 (6)	C(35)	0.460 (5)	0.2085 (34)	0.311 (5)	26.9 (34)
C(7)	0.174 (2)	0.2055 (13)	0.143 (2)	6.0 (8)	C(45)	0.281 (3)	0.1333 (25)	0.438 (3)	15.9 (18)
C(8)	0.299 (2)	0.2009 (18)	0.146 (2)	9.5 (12)	C(55)	0.247 (3)	0.6474 (30)	0.013 (4)	17.0 (23)
C(9)	0.307 (2)	0.1212 (13)	0.236 (2)	5.7 (7)	C(65)	0.356 (3)	0.1228 (24)	0.450 (3)	15.5 (19)

atom	B(1,1)	B(2,2)	B(3,3)	B(1,2)	B(1,3)	B(2,3)
Rh1	0.00243 (6)	0.00157 (3)	0.00264 (5)	0.0002 (1)	0.0000 (2)	0.00006 (10)
Rh2	0.00160 (4)	0.00149 (3)	0.00244 (5)	0.0003 (1)	0.0002 (2)	−0.00017 (9)
Mn1	0.0093 (3)	0.00188 (9)	0.0035 (2)	0.0011 (3)	−0.0002 (5)	−0.0014 (2)
Mn2	0.0049 (2)	0.00198 (9)	0.0032 (2)	−0.0005 (2)	0.0011 (3)	−0.0006 (2)

[a] The form of the anisotropic thermal parameter is $\exp[-(B(1,1)h^2 + B(2,2)k^2 + B(3,3)l^2 + B(1,2)hk + B(1,3)hl + B(2,3)kl)]$.

were found to be slightly shorter, averaging 2.815 (15) Å. Due to the obvious gross differences between $[Rh_2(TM4\text{-bridge})_4Mn_2(CO)_{10}]^{2+}$ and the other compounds mentioned here (i.e. different metal atoms and different ligation) further discussion of the variations in these metal–metal distances is probably not warranted.

The coordination sphere about the Rh atoms is completed by the four bridging TM4-bridge ligands, giving each Rh atom pseudooctahedral microsymmetry (a view of the coordination core $Rh_2(CN)_8Mn_2(CO)_{10}$ is given in Figure 3). The two $Rh(CN)_4$ planes are both nearly planar (Table VI) and coplanar with each other, the plane normals making an angle of 2.6° with each other. The two $Rh(CN)_4$ units are twisted away from the eclipsed conformation with respect to one another by a 25 (3)° angle. Similarly, in $Rh_2(TM4\text{-bridge})_4(PF_6)_2\cdot CH_3CN$, the $Rh(CN)_4$ units are twisted by a 31 (1)° angle.[4] The Rh–C bond lengths of 1.95 (6) are quite comparable to those found in previously determined Rh isocyanide complexes. For example, in the $Rh_4(bridge)_8Cl^{5+}$ ion,[12] Rh–C bond lengths are 1.96 (6) Å, as are those in $Rh_2(bridge)_4^{2+}$[11] and $Rh_2(TM4\text{-bridge})_4^{2+}$[4] while in the $Rh_2(bridge)_4Cl_2^{2+}$ ion[15] they are 1.99 (1) Å. The average C≡N bond length of 1.14 (8) Å is also similar to that found in the parent ion $Rh_2(TM4\text{-bridge})_4^{2+}$[4] of 1.16 (1) Å.

The average C–C bond lengths and C–C–C bond angles found in the ligand chains (1.55 (9) Å and 112 (7)°, respectively) are close to those found for the previously determined parent ion $Rh_2(TM4\text{-bridge})_4^{2+}$[11] (1.54 (3) Å and 112 (11)°).

The coordination core of each Mn atom is also close to pseudooctahedral, with the $Mn(CO)_4$ units nearly planar (Table VI). The deviations from planarity in the $Mn(CO)_4$

(15) Mann, K. R.; Bell; R. A.; Gray, H. B. *Inorg. Chem.* **1979**, *18*, 2671–2673.

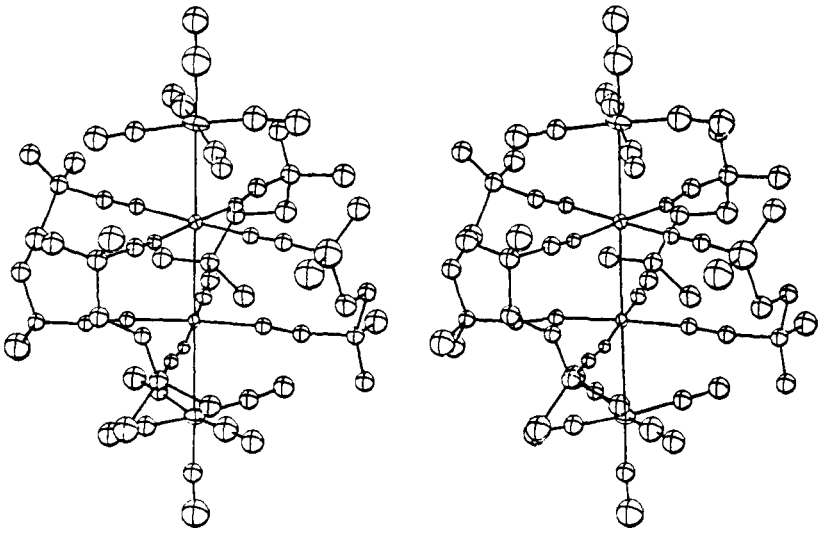

Figure 2. ORTEP stereoview of the $[Rh_2(TM4\text{-bridge})_4Mn_2(CO)_{10}]^{2+}$ dication perpendicular to the M–M bond vectors.

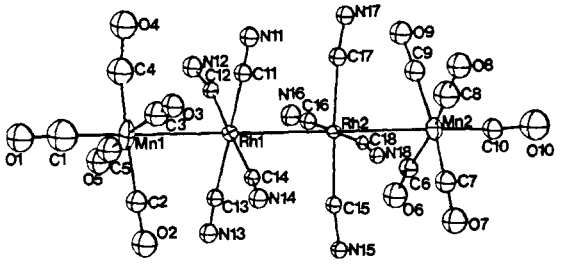

Figure 3. ORTEP drawing of the $Rh_2(CN)_8Mn_2(CO)_{10}$ coordination core.

Table III. Selected Bond Lengths (Å) for the $[Rh_2(TM4\text{-bridge})_4Mn_2(CO)_{10}]^{2+}$ Cation[a]

	M–M		
Rh1-Mn1	2.905 (5)	Rh1-Rh2	2.922 (2)
Rh2-Mn2	2.883 (4)		
	Rh–C		
Rh1-C11	1.87 (3)	Rh2-C15	1.92 (2)
Rh1-C12	1.97 (2)	Rh2-C16	1.91 (2)
Rh1-C13	2.05 (3)	Rh2-C17	1.99 (2)
Rh1-C14	1.99 (2)	Rh2-C18	1.96 (2)
	C≡N		
C11-N11	1.17 (3)	C15-N15	1.19 (2)
C12-N12	1.23 (3)	C16-N16	1.28 (3)
C13-N13	1.05 (3)	C17-N17	1.10 (2)
C14-N14	1.07 (3)	C18-N18	1.08 (2)
	C–C and C–N		
C-C[b]	1.55 (9)[c]	C-N[b]	1.49 (6)[c]
	Mn–C(equatorial)		
Mn1-C2	1.79 (3)	Mn2-C6	1.79 (3)
Mn1-C3	1.89 (4)	Mn2-C7	1.66 (3)
Mn1-C4	1.78 (4)	Mn2-C8	1.58 (4)
Mn1-C5	1.89 (4)	Mn2-C9	1.88 (3)
	Mn–C(apical)		
Mn1-C1	1.76 (5)	Mn2-C2	1.71 (3)
	C≡O(equatorial)		
C2-O2	1.14 (3)	C6-O6	1.16 (3)
C3-O3	1.11 (3)	C7-O7	1.27 (3)
C4-O4	1.22 (4)	C8-O8	1.36 (4)
C5-O5	1.14 (4)	C9-O9	1.17 (3)
	C≡O(apical)		
C1-O1	1.26 (5)	C10-O10	1.31 (3)

[a] The numbers in parentheses are the estimated standard deviations of the last significant figure. [b] Average values. [c] The standard deviation given in parentheses following an average bond distance or angle, $\bar{x}$, is defined as $\sigma = [\Sigma_i(x_i - \bar{x})^2/(N-1)]^{1/2}$, where N is the number of observations, x_i.

Table IV. Selected Bond Angles (Deg) for the $[Rh_2(TM4\text{-bridge})_4Mn_2(CO)_{10}]^{2+}$ Cation[a]

	Mn–Rh–Rh		
Mn1-Rh1-Rh2	179.3 (1)	Mn2-Rh2-Rh1	177.0 (1)
	M–Rh1–C		
Mn1-Rh1-C11	91.3 (7)	Rh2-Rh1-C11	89.4 (7)
Mn1-Rh1-C12	91.6 (7)	Rh2-Rh1-C12	88.2 (7)
Mn1-Rh1-C13	88.9 (7)	Rh2-Rh1-C13	90.4 (7)
Mn1-Rh1-C14	90.8 (6)	Rh2-Rh1-C14	89.4 (6)
	Rh–C≡N		
Rh1-C11-N11	174 (2)	Rh2-C15-N15	174 (2)
Rh1-C12-N12	170 (2)	Rh2-C16-N16	178 (2)
Rh1-C13-N13	174 (2)	Rh2-C17-N17	172 (3)
Rh1-C14-N14	170 (2)	Rh2-C18-N18	170 (2)
	Rh–Mn–C(equatorial)		
Rh1-Mn1-C2	87 (1)	Rh2-Mn2-C6	86 (1)
Rh1-Mn1-C3	83 (1)	Rh2-Mn2-C7	86 (1)
Rh1-Mn1-C4	88 (1)	Rh2-Mn2-C8	88 (1)
Rh1-Mn1-C5	85 (1)	Rh2-Mn2-C9	88 (1)
	M–Rh2–C		
Mn2-Rh2-C15	88.4 (7)	Rh1-Rh2-C15	92.1 (7)
Mn2-Rh2-C16	87.5 (6)	Rh1-Rh2-C16	89.5 (7)
Mn2-Rh2-C17	89.1 (8)	Rh1-Rh2-C17	90.5 (8)
Mn2-Rh2-C18	90.4 (5)	Rh1-Rh2-C18	92.5 (5)
	C–N≡C		
C11-N11-C54	174 (3)	C15-N15-C24	172 (2)
C12-N12-C41	168 (2)	C16-N16-C44	172 (3)
C13-N13-C21	173 (2)	C17-N17-C51	171 (3)
C14-N14-C34	165 (3)	C18-N18-C31	175 (2)
	Mn–C≡O(equatorial)		
Mn1-C2-O2	177 (3)	Mn2-C6-O6	175 (2)
Mn1-C3-O3	173 (3)	Mn2-C7-O7	178 (2)
Mn1-C4-O4	159 (3)	Mn2-C8-O8	178 (2)
Mn1-C5-O5	177 (3)	Mn2-C9-O9	175 (3)
	Rh–Mn–C(apical)		
Rh1-Mn1-C1	176 (2)	Rh2-Mn2-C10	178 (1)
	Mn–C≡O(apical)		
Mn1-C1-O1	168 (4)	Mn2-C10-O10	173 (2)

[a] The numbers in parentheses are the estimated standard deviations of the last significant figure.

units, however, are definitely larger than those of the $Rh(CN)_4$ planes, possibly reflecting the fact that the Mn–CO bond angles are more easily distorted since the carbonyl oxygen atoms are not bound at both ends as are the nitrogen atoms in the Rh–CNR units. The planes defined by the $Mn(CO)_4$ groups are also within 5° of being parallel to the $Rh(CN)_4$ planes.

Table V. Bond Lengths (Å) in the Anions and the Acetone Solvate[a]

	PF_6^-		
P1-F11	1.57 (2)	P2-F21	1.63 (3)
P1-F12	1.49 (2)	P2-F22	1.54 (3)
P1-F13	1.55 (2)	P2-F23	1.38 (6)
P1-F14	1.51 (2)	P2-F24	1.49 (6)
P1-F15	1.59 (3)	P2-F25	1.65 (5)
P1-F16	1.60 (3)	P2-F26	1.54 (5)
	CO-C		
C1-C2	1.8 (1)	C4-C5	1.47 (7)
C1-C3	1.9 (1)	C4-C6	1.40 (6)
	C=O		
C1-O1	1.0 (1)	C4-O2	1.25 (6)

[a] The numbers in parentheses are the estimated standard deviations of the last significant figure.

Table VI. Weighted Least-Squares Planes[a]

atom	dev, Å	atom	dev, Å
	$Rh1(CN)_4$		
C11	0.02 (3)	N13	−0.02 (2)
N11	−0.04 (2)	C14	0.04 (3)
C12	0.04 (3)	N14	0.10 (2)
N12	−0.10 (2)	Rh1	0.001 (1)
C13	−0.02 (3)		
	$Rh2(CN)_4$		
C15	−0.04 (3)	N17	−0.21 (2)
N15	−0.18 (2)	C18	−0.02 (2)
C16	−0.04 (3)	N18	−0.03 (2)
N16	−0.05 (3)	Rh2	0.006 (2)
C17	−0.04 (3)		
	$Mn1(CO)_4$		
C2	0.04 (3)	O4	0.15 (3)
O2	0.14 (3)	C5	0.14 (4)
C3	0.15 (4)	O5	0.25 (2)
O3	0.21 (2)	Mn1	−0.045 (5)
C4	0.05 (4)		
	$Mn2(CO)_4$		
C6	0.12 (3)	O8	0.19 (2)
O6	0.15 (2)	C9	0.02 (3)
C7	0.09 (3)	O9	0.14 (2)
O7	0.17 (2)	Mn2	−0.030 (4)
C8	0.11 (4)		

[a] Positive deviation is toward cation center. The numbers in parentheses are the estimated standard deviations of the last significant figure.

The Mn–C bonds average 1.78 (11) Å for the four equatorial carbonyls and 1.74 (4) Å for the two apical carbonyls. In $Mn_2(CO)_{10}$,[13] these distance are both longer (1.831 (15) and 1.792 (14) Å, respectively), possibly due to slightly stronger Mn–C bonding in the Rh derivative.[16]

The C≡O bonds of the cation (1.20 (8) (equatorial) and 1.29 (4) Å (apical)) are both found to be lengthened relative to the $Mn_2(CO)_{10}$ values[13] which are 1.157 (16) and 1.151 (16) Å, respectively. Although these values for the C≡O bond lengths are quite long, we feel that they are probably not significant,[16] due to insufficient resolution and/or severe thermal motion found in these atoms.

Photochemical Reactions. We have carried out several preliminary experiments to ascertain the mechanism for both the photochemical formation and decomposition of the

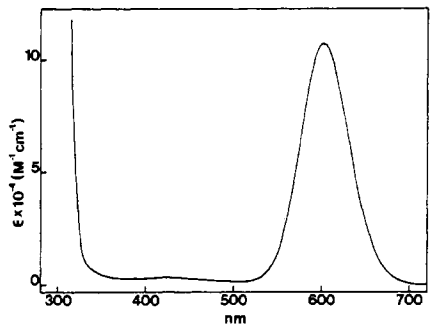

Figure 4. Visible absorption spectrum of a 1.47×10^{-4} M solution of $[Rh_2(TM4\text{-bridge})_4Mn_2(CO)_{10}](PF_6)_2$ in degassed acetone at room temperature. The cell path length is 0.115 cm.

$[Rh_2(TM4\text{-bridge})_4Mn_2(CO)_{10}]^{2+}$ ion. Photolysis of degassed solutions of $Mn_2(CO)_{10}$ (2.6×10^{-3} M) and $Rh_2(TM4\text{-bridge})_4^{2+}$ (1.2×10^{-3} M) at 405 and at 546 nm have been carried out. These two wavelengths were chosen since the absorption of radiation at 405 nm is primarily (~90%) due to the $d\pi \rightarrow \sigma^*$ transition[2] in $Mn_2(CO)_{10}$ and at 546 nm due almost entirely to the MLCT band of $Rh_2(TM4\text{-bridge})_4^{2+}$.[4,16] The results show that the quantum yield ϕ for the formation of $[Rh_2(TM4\text{-bridge})_4Mn_2(CO)_{10}]^{2+}$ at 405 nm is 0.20 (1) a factor of nearly 700 larger than the quantum yield at 546 nm ($\phi = 2.9\ (7) \times 10^{-4}$). We interpret these results as being consistent with the production of an excited state of $Mn_2(CO)_{10}$ as the primary step in the formation of $[Rh_2(TM4\text{-bridge})_4Mn_2(CO)_{10}]^{2+}$. The finite value of $\phi_{formation}$ at 546 nm could be due to either a small amount of impurity light in our interference filter isolated 546 nm radiation, a small amount of absorption due to $Mn_2(CO)_{10}$ at 546 nm, or the indirect formation of an excited state of $Mn_2(CO)_{10}$ by a sensitization mode involving either energy or electron transfer from $[Rh_2(TM4\text{-bridge})_4^{2+}]^*$ to $Mn_2(CO)_{10}$. At this time, we favor a small amount of absorption due to $Mn_2(CO)_{10}$ at 546 nm as the cause of the observed reaction at 546 nm. On the basis of the evidence that excitation of either the $\sigma \rightarrow \sigma^*$ band at higher energy or the $d\pi \rightarrow \sigma^*$ band of $Mn_2(CO)_{10}$ results in efficient metal–metal bond cleavage to give reactive $Mn(CO)_5$ radicals,[3] we favor eq 1 and 2 as a pathway for the formation

$$Mn_2(CO)_{10} \xrightarrow{h\bar{\nu}} 2Mn(CO)_5 \quad (1)$$

$$Mn(CO)_5 + Rh_2(TM4\text{-bridge})_4^{2+} \rightarrow [Rh_2(TM4\text{-bridge})_4Mn(CO)_5]^{2+} \quad (2)$$

of $[Rh_2(TM4\text{-bridge})_4Mn_2(CO)_{10}]^{2+}$ upon 405-nm irradiation[17] followed by either eq 3a or 3b.

$$Mn(CO)_5 + [Rh_2(TM4\text{-bridge})_4Mn(CO)_5]^{2+} \rightarrow [Rh_2(TM4\text{-bridge})_4Mn_2(CO)_{10}]^{2+} \quad (3a)$$

$$Mn_2(CO)_{10} + [Rh_2(TM4\text{-bridge})_4Mn(CO)_5]^{2+} \rightarrow [Rh_2(TM4\text{-bridge})_4Mn_2(CO)_{10}]^{2+} \quad (3b)$$

Clearly, more experiments are needed to differentiate the relative contributions of steps 3a and 3b in the formation of $[Rh_2(TM4\text{-bridge})_4Mn_2(CO)_{10}]^{2+}$, although we favor step 3a

(16) We view with some suspicion both the short Mn—C bond lengths and the long C≡O bond lengths, especially those for the apical carbonyls. The temperature factors for the carbonyl carbon and oxygen atoms are significantly larger than those for the light atoms in the bridging TM4-bridge ligands. Also, the $\bar{\nu}$(CO) IR stretching frequencies are not out of line with those found in other $Mn(CO)_5X$ compounds, with presumably "normal" Mn—C and C≡O bond lengths: Kaesz, H. D.; Bau, R.; Hendrickson, D. N.; Smith, J. M. *J. Am. Chem. Soc.* **1967**, *89*, 2844–2851.

(17) Brown and co-workers have found that $Mn(CO)_5$ radicals are extremely labile in the presence of nucleophiles: Byers, B. H.; Brown, T. L. *J. Am. Chem. Soc.* **1975**, *97*, 947–948; **1976**, *98*, 3160–3166; **1977**, *99*, 2527–2532. Although we have no evidence for dissociation of $Mn(CO)_5$ in acetone solutions, we recognize the possibility that the actual radical species reacting with $Rh_2(TM4\text{-bridge})_4^{2+}$ might well be $Mn(CO)_4$(acetone). The tetranuclear ion produced after successive reactions, $[Rh_2(TM4\text{-bridge})_4Mn_2(CO)_8(acetone)_2]^{2+}$, could then undergo substitution by two molecules of carbon monoxide to give the final product ion.

over 3b since 3b is a radical chain propagation step, which, if operational, would probably give a larger quantum yield than is observed.

The visible absorption spectrum of a 1.47×10^{-4} M solution of $[Rh_2(TM4\text{-bridge})_4Mn_2(CO)_{10}]^{2+}$ at room temperature in acetone solution is shown in Figure 4. The striking feature in the absorption spectrum of this compound is the intense band ($\epsilon = 106000\ M^{-1}\ cm^{-1}$) centered at 600 nm. By analogy to a similar band found in the $[Rh_2(bridge)_4]_2^{6+}$ ion,[12] we assign this band to the lowest energy allowed $\sigma \rightarrow \sigma^*$ transition (vide infra).

To test our initial hypothesis that excitation of $\sigma \rightarrow \sigma^*$ transitions in multinuclear linear clusters might generate novel, reactive transition-metal fragments, we have also attempted the photolysis of the tetranuclear $[Rh_2(TM4\text{-bridge})_4Mn_2(CO)_{10}]^{2+}$ ion at 632.8 nm in acetone solution by using a 4-mW HeNe laser. We find that in air-saturated solutions, $[Rh_2(TM4\text{-bridge})_4Mn_2(CO)_{10}]^{2+}$ slowly ($\phi = 0.02$ (1)) decomposes cleanly to give $Rh_2(TM4\text{-bridge})_4^{2+}$ and an undetermined Mn complex. However, in degassed solutions, the decomposition quantum yield is much smaller ($\phi = 5\ (5) \times 10^{-5}$) suggesting either that the tetranuclear ion is virtually stable under irradiation under these conditions or that rapid recombination of photolysis products to regenerate $[Rh_2(TM4\text{-bridge})_4Mn_2(CO)_{10}]^{2+}$ occurs. Since the reaction of two $Mn(CO)_5$ radicals to reform $Mn_2(CO)_{10}$ is quite rapid (at least in hexane $k = 3.9 \times 10^9\ M^{-1}\ s^{-1}$ at 20 °C)[18] it appears that the photochemically induced bond cleavage of $[Rh_2(TM4\text{-bridge})_4Mn_2(CO)_{10}]^{2+}$ to give $[Rh_2(TM4\text{-bridge})_4Mn(CO)_5]^{2+}$ and $Mn(CO)_5$ is not facile at 632.8 nm. These results contrast with those obtained for the tetranuclear $[Rh_2(bridge)_4]_2^{6+}$ ion,[19] which exhibits much more efficient bond rupture in aqueous H_2SO_4 solutions to give two $Rh_2(bridge)_4^{3+}$ fragments with a quantum yield of $\phi = 0.02$ by using light of comparable energy.

Both the relative photostability of $[Rh_2(TM4\text{-bridge})_4Mn_2(CO)_{10}]^{2+}$ and the photoinstability of $[Rh_2(bridge)_4]_2^{6+}$ are explicable in terms of a simple molecular orbital treatment of the metal–metal bonding based on a linear tetranuclear system utilizing the d_{z^2} orbital on each metal atom to form four MO's. The lowest $\sigma \rightarrow \sigma^*$ type transition in such a system, which would contain six electrons, excites an electron from an orbital which is bonding with respect to the two inner metal atoms and antibonding with respect to the outer atoms to an orbital which is antibonding with respect to all the metal–metal interactions. Thus the most significant changes in the metal–metal bond framework cause the bond between the inner two metal atoms to weaken. However, in the $[Rh_2(TM4\text{-bridge})_4Mn_2(CO)_{10}]^{2+}$ ion this weakened RhRh bond is restrained from breaking by the four bridging TM4-bridge ligands. On the other hand, in $[Rh_2(bridge)_4]_2^{6+}$ the weakened central RhRh bond is not restrained so that homolytic cleavage into two $Rh_2(bridge)_4^{3+}$ units can readily occur.

Further mechanistic experiments including flash photolysis experiments are in progress to further clarify both the mechanism of formation and decomposition of the $[Rh_2(TM4\text{-bridge})_4Mn_2(CO)_{10}]^{2+}$ ion.

Acknowledgment. Support of this research through a Du Pont Young Faculty Grant and a University of Minnesota Faculty Summer Research Appointment are gratefully acknowledged. We wish to thank Dr. D. Britton, Dr. L. Pignolet, and Mr. M. McGuiggan for their expert assistance in carrying out the crystal structure determination. We also thank the NSF for partial support of our X-ray diffraction and structure-solving equipment (No. NSF CHE7728505) and our Cary 17-D spectrophotometer (No. CHE 78-23857).

Registry No. $[Rh_2(TM4\text{-bridge})_4Mn_2(CO)_{10}](PF_6)_2 \cdot 2(CH_3)_2CO$, 75198-28-6; $Rh_2(TM4\text{-bridge})_4(PF_6)_2$, 73367-42-7; $Mn_2(CO)_{10}$, 10170-69-1.

Supplementary Material Available: Table of observed and calculated structure factors (12 pages). Ordering information is given on any current masthead page.

(18) Hughey, J. L., IV; Anderson, C. P.; Meyer, T. J. *J. Organomet. Chem.* **1977**, *125*, C49–C52.
(19) Miskowski, V. M.; Sigal, I. S.; Mann, K. R.; Gray, H. B.; Milder, S. J.; Hammond, G. S.; Ryason, P. R. *J. Am. Chem. Soc.* **1979**, *101*, 4383–4385.

Contribution from the Institute of Molecular Biology and Department of Chemistry, National Tsing Hua University, Hsinchu, Taiwan, Republic of China

Crystal and Molecular Structure of (1,1,4,4-Tetrafluoro-2-*tert*-butyl-1,4-disilabut-2-ene)molybdenum(II) Pentacarbonyl

T. H. HSEU,*[1a] YUN CHI,[1b] and CHAO-SHIUAN LIU*[1b]

Received June 25, 1980

(1,1,4,4-Tetrafluoro-2-*tert*-butyl-1,4-disilabut-2-ene)molybdenum(II) pentacarbonyl has been prepared photochemically by reaction of 3-*tert*-butyl-1,1,2,2-tetrafluoro-1,2-disilacyclobutene with molybdenum hexacarbonyl in pentane. The crystal structure was determined by X-ray diffraction. The crystal is triclinic, of space group $P\bar{1}$, with $Z = 2$; $a = 12.710$ (3) Å, $b = 10.236$ (2) Å, $c = 7.242$ (5) Å, $\alpha = 86.53$ (3)°, $\beta = 93.78$ (3)°, $\gamma = 70.65$ (2)°, and $D_{calcd} = 1.568$ g cm^{-3}. The structure was solved by heavy-atom methods and refined by full-matrix least squares with the use of anisotropic temperature factors to an R value of 0.059 for 2897 independent reflections. The central molybdenum atom is seven-coordinated with a pentagonal-bipyramidal environment. The pentagonal base contains the disilabutene ligand and three carbonyl groups. The average bonding distances are 2.041 (13) Å for Mo–C and 2.605 (3) Å for Mo–Si. The five-membered molybdodisilabutene ring is rather strained with endocyclic silicon and carbon valence angles substantially greater and smaller than their tetrahedral and trigonal ideal ones, respectively. The transannular Si···Si distance is 2.861 Å, which is substantially shorter than the sum of van der Waals radii, suggesting there might be direct silicon–silicon cross-ring interaction.

Introduction

A recent interest in the study of organosilicon compounds has been focused on the reactions of vinyldisilanes.[2-5] Under photochemical conditions these compounds react in such a way that intermediates involving a silicon–carbon double bond have

(1) (a) Institute of Molecular Biology. (b) Department of Chemistry.

(2) H. Sakurai, Y. Kamiyama, and Y. Nakadaira, *J. Am. Chem. Soc.*, **98**, 7424 (1976).

0020-1669/81/1320-0199$01.00/0